Electronic Supplementary Material (ESI) for Physical Chemistry Chemical Physics.

Ultralow lattice thermal conductivity and dramatically enhanced thermoelectric properties of monolayer InSe induced by external electric field

Zheng Chang[1], Kunpeng Yuan[1], Zhehao Sun[1], Xiaoliang Zhang[1*], Yufei Gao[1*], Guangzhao Qin[2*], Dawei Tang[1*]

[1]Key Laboratory of Ocean Energy Utilization and Energy Conservation of Ministry of Education, School of Energy and Power Engineering, Dalian University of Technology, Dalian 116024, China.

[2]State Key Laboratory of Advanced Design and Manufacturing for Vehicle Body, College of Mechanical and Vehicle Engineering, Hunan University Changsha 410082, China

[*]Corresponding author. Email: zhangxiaoliang@dlut.edu.cn, gaoyufei@dlut.edu.cn, gzqin@hnu.edu.cn and dwtang@dlut.edu.cn

To overcome the atomic motions of the first and last phonon branches of indistinguishable, we added the corresponding vibrational modes of the first and last phonon branches for 2D InSe and shown in Fig. S1. It can be clearly observed that the first and last phonon branches represent vibration modes near the Γ point for the ZA branch and the ZO branch at the electric field of 0 and 0.3 V/Å, respectively.

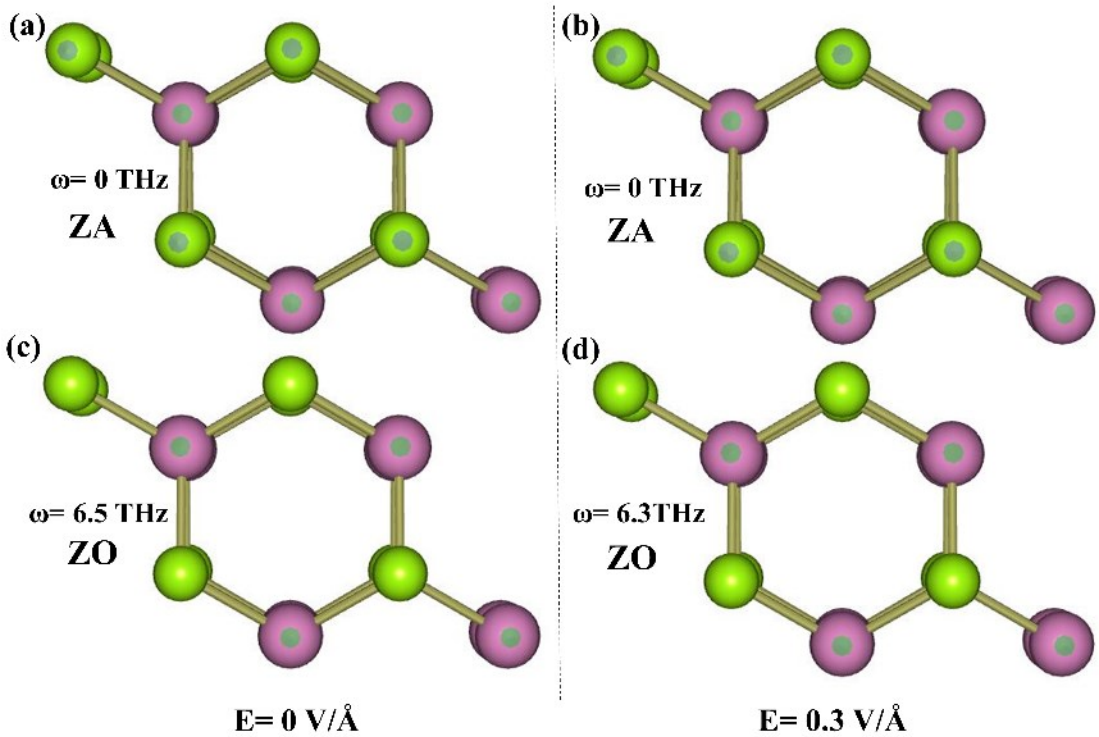

Fig. S1 (a) and (c) represent vibration modes near the Γ point for the *out-of-plane* acoustic phonon branch (ZA) and the *out-of-plane* optical phonon (ZO) branch without electric field. (c) and (d) represent vibration modes near the Γ point for the *out-of-plane* acoustic phonon branch (ZA) and the *out-of-plane* optical phonon (ZO) branch at the electric field of 0.3 V/Å.

We have added and the vdW density functionals (optB86b, optB88, optPBE revPBE and vdW-DF2) to calculate phonon dispersion curves of 2D InSe along the high symmetric path in the Brillouin zone, shown in the Fig. S2. It can be noticed that all the phonon modes show positive frequencies under the vdW density functionals which can prove the dynamic stability in our structure. Meanwhile, according to the comparison of different functionals of 2D InSe at the external electric field of 0 0.3 V/Å, its phonon dispersion curves of three acoustic phonon branches are not changed, while the optical phonons exist some slight decreases.

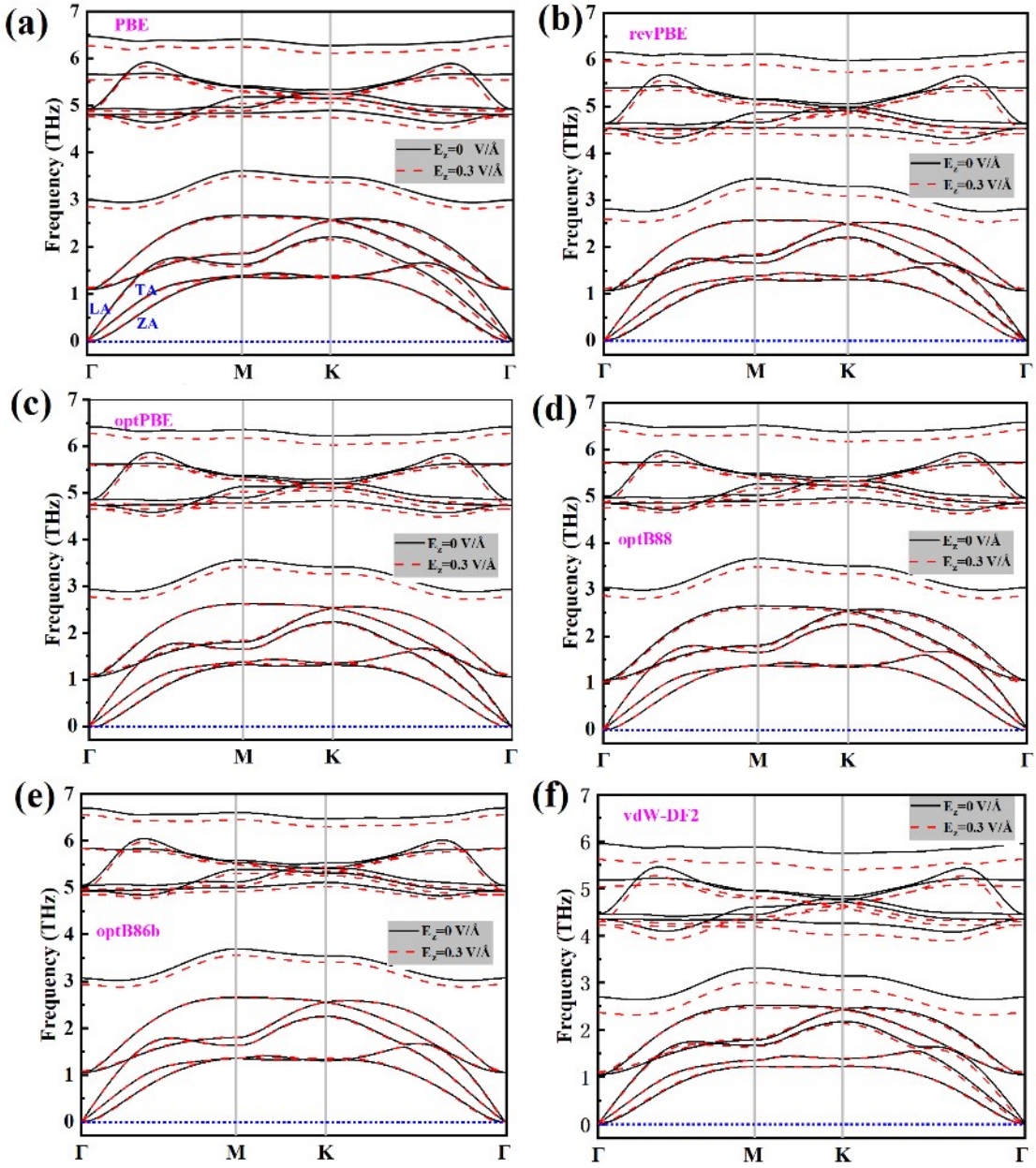

Fig. S2. Comparison of the phonon dispersion curves of 2D InSe with (0.3 V/Å) and without electric fields applied.

As we known, *ab initio* molecular dynamics (AIMD) simulation is widely employed in quantifying the thermodynamic stability of materials. Here, we have performed the AIMD simulations at three different temperatures cases (300, 500 and 700 K) with NVT ensemble (requiring constant number, volume and temperature), lasting for 6.7 ps with a time interval of 1 fs to assess the thermodynamic stability of 2D InSe. The 5×5×1 supercell was used by using the Nosé–Hoover thermostat.[1]

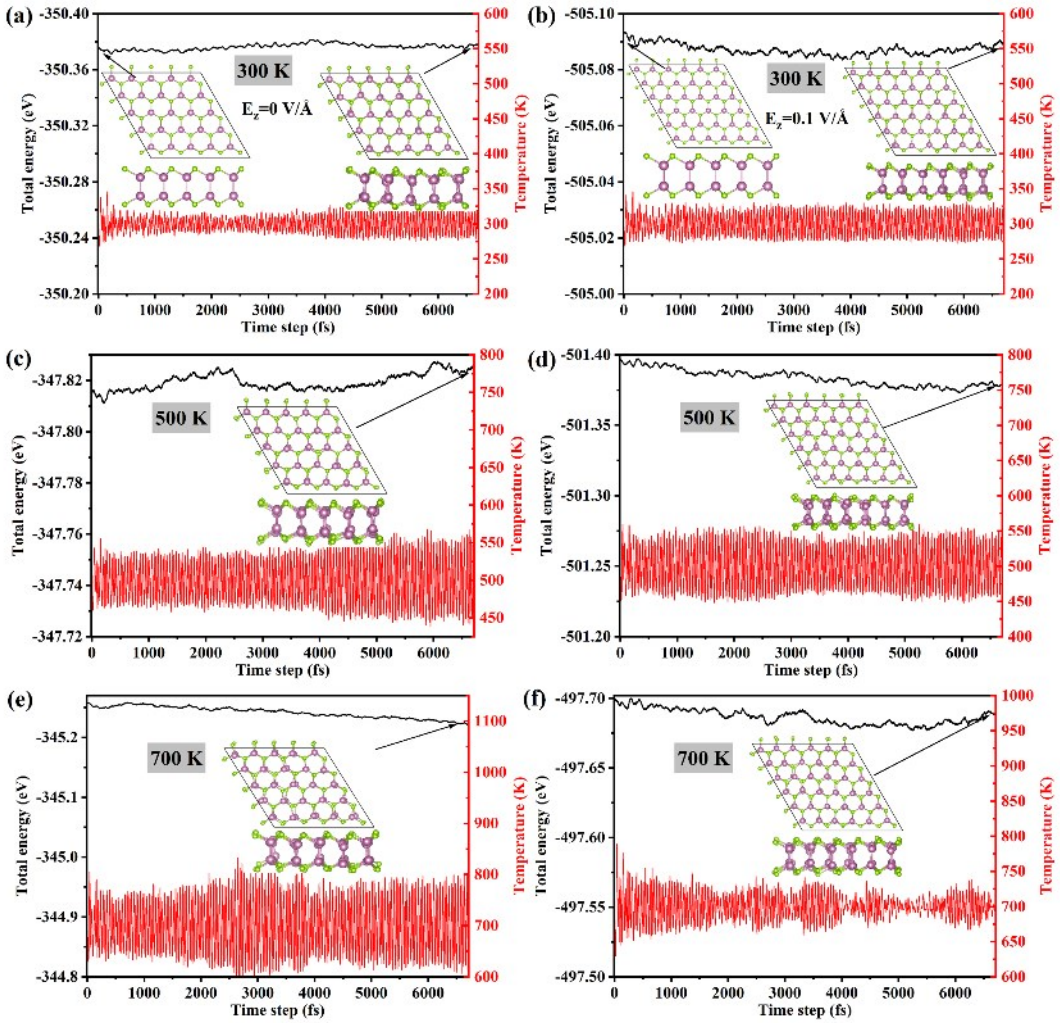

Fig. S3. Total energy and Temperature fluctuation with respect to time in AIMD simulation under without (a-c-e) and with external electric field (E_z=0.1 V/Å) cases (b-d-f) for 2D InSe. The final snapshot of the atomic configuration were obtained at temperatures (T=300, 500 and 700K).

As shown in Fig. S3, it can be noticed that the total energy of 2D InSe fluctuates in a narrow range and no bonds are broken under two representative electric fields cases. As a result, these structures could be thermodynamically feasible as its equilibrium structure at 300 K up to 700 K. It has been reported that if a material is dynamically stable, we need to evince that it cannot undergo any structural changes (no phase transition occurring).[2] To accurately describe structural changes of 2D InSe, we calculated the snapshots of the AIMD simulated trajectories at 300 K and 700 K under the external electric fields of 0 and 0.1 V/Å, as plotted in Fig. S4 (a-d). On the basis of

the trajectories, it can be clearly seen that the average radii of the atomic displacements at 700 K are larger than those at 300 K for all cases. Meanwhile, the trajectories can indicate that In and Se atoms are constrained to around their equilibrium position and further investigate not a phase transition under an external electric field. We have calculated the energy above the convex hull of 2D InSe, which can predict the thermodynamic stability of a material system, as shown in Fig. S4 (e). Our results are confirmed and in good agreement with the previous theoretical calculations.[2]

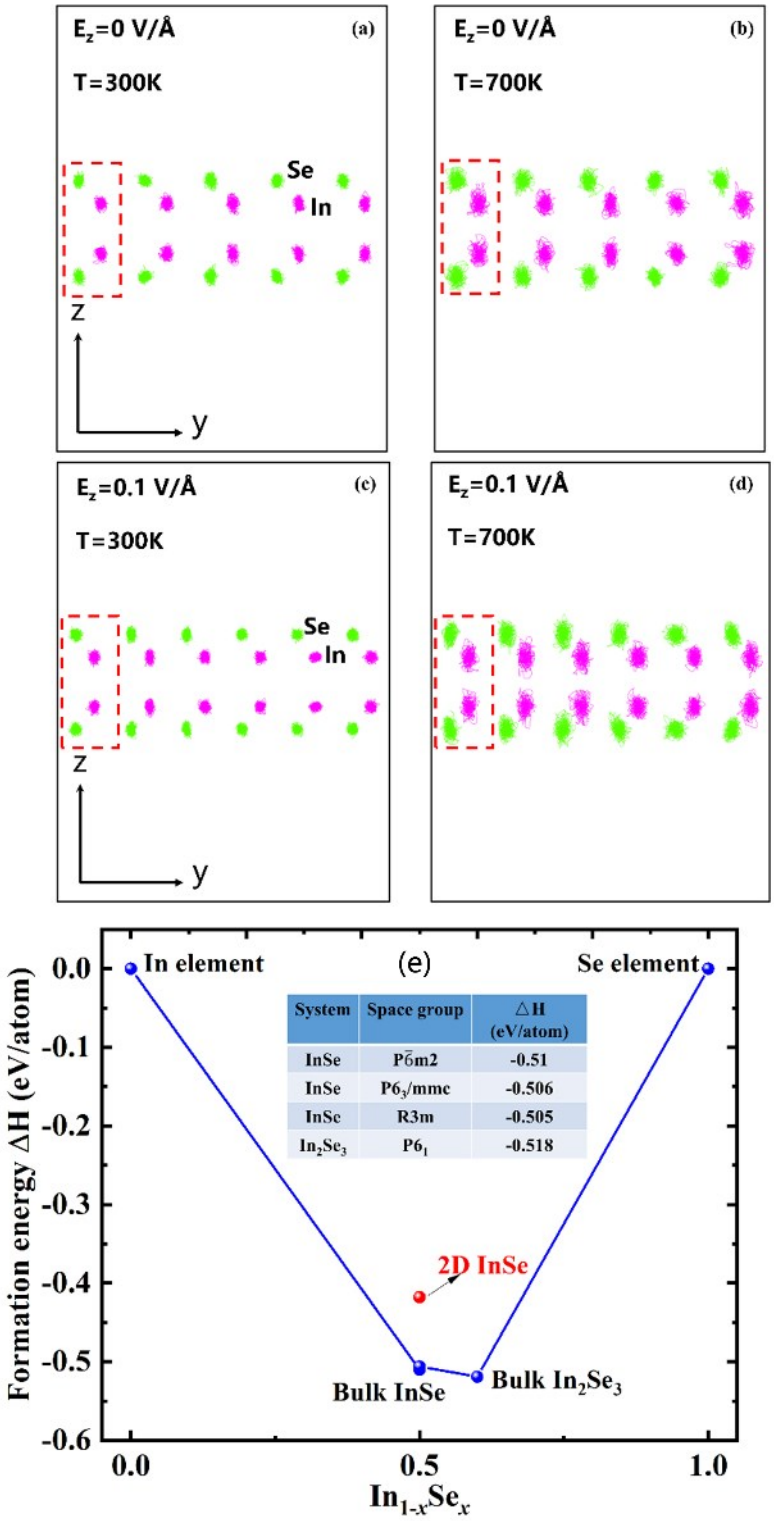

System	Space group	△H (eV/atom)
InSe	$P\bar{6}m2$	-0.51
InSe	$P6_3/mmc$	-0.506
InSe	R3m	-0.505
In_2Se_3	$P6_1$	-0.518

Fig. S4 (a) and (b) plotted the AIMD simulated trajectory of atoms in the *y-z* plane of 2D InSe at 300 K and 700 K without electric field, respectively. (c) and (d) plotted the AIMD simulated trajectory of atoms in the *y-z* plane of 2D InSe at 300 K and 700 K at the electric field of 0.1 V/Å, respectively. (e) Energy above the convex hull for $In_{1-x}Se_x$. The convex hull as defined by the bulk phases is presented by the blue solid lines. Blue spheres and red sphere denote bulk binary reference phases and 2D InSe (in this work), respectively. The inset shows our calculated the formation energy for different bulk $In_{1-x}Se_x$ phases.

As we discussed, the cutoff radius can be directly determined to get satisfactory lattice thermal conductivity results based on the analysis of harmonic IFCs.[3] To quantify the strength of interatomic interactions for 2D InSe, traces of interatomic force constant (IFC) tensors are normalized by the trace values of the self-interacting IFC tensor.[4] Note that the RTA method slightly underestimates the κ_l but the variation trend still holds.

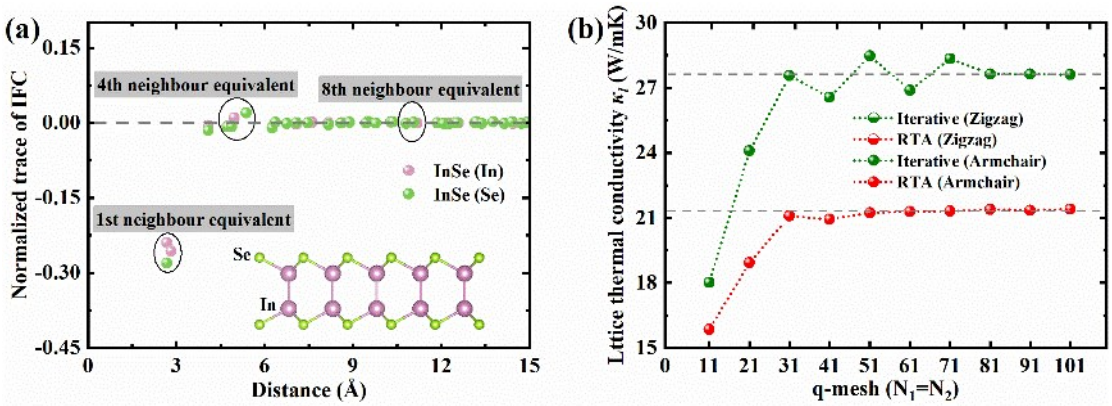

Fig. S5. (a) Normalized trace of interatomic force constant tensors versus atomic distances for 2D InSe. (b) Intrinsic and relaxation time approximation (RTA) lattice thermal conductivity of 2D InSe as a function of different numbers of q-mesh at 300 K.

It can be clearly seen that the ELF values only slightly changes with the increase of electric fields. Furthermore, the electronic charges are mainly localized near In and Se bonds, indicating the stronger covalent bonding between In and Se atoms. It is understood that the stronger covalent bonding is usually difficult to break, and thus the external electric fields in our work can not break 2D InSe crystal symmetry.

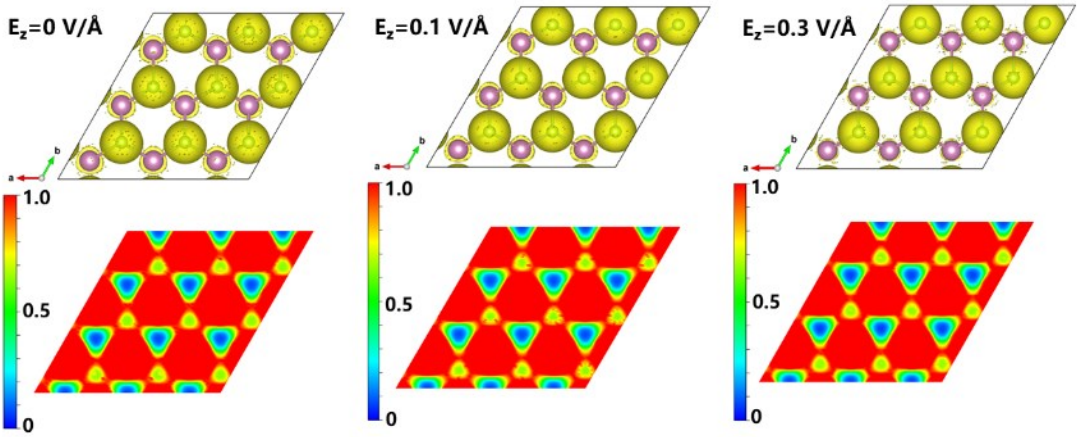

Fig. S6. The ELF iso-surface and its value of slice perpendicular to (0 0 1) direction of 2D InSe (3×3×1 supercells) at the electric fields of 0. V/Å, 0.1 V/Å and 0.3 V/Å, respectively.

As reported in the previous work,[5] a tuning thermoelectric performance method by the external electric field applied is easy to be realized in practice. Through DFT calculation coupled with the post-processing tool VASPKIT,[6] we obtain the Born effective charge and dielectric constant tensor under different external electric fields. The values of the parameters of 2D InSe without electric field are close to those in the literature.[7 8] The 2D InSe crystal structure in the text, having hexagonal symmetry, has two non-zero diagonal components of the dielectric tensor, namely, $\varepsilon_{xx}(\varepsilon_{xx} = \varepsilon_{yy})$ and ε_{zz}. The two dielectric tensors were depicted in Table. S1 and can be obtained from the dielectric function based on the Ehrenreich-Cohen formula[9] and the effective medium theory,[10] expressed by $\varepsilon_{xx} = 1 + \frac{L}{d}[\varepsilon_{SL} - 1]$ and $\frac{1}{\varepsilon_{zz}} = 1 + \frac{L}{d}\left[\frac{1}{\varepsilon_{SL}} - 1\right]$. According to the Ehrenreich-Cohen formula, ε_{SL} can also be obtained based on the following equation ($\varepsilon_{SL} = 1 + \frac{2e^2\hbar^2}{\varepsilon_0 m^2} \frac{1}{LS} \sum_{c,v} \sum_{k} \frac{|<c|p_j|v>|^2}{[\varepsilon_c - \varepsilon_v]^2} \times \sum_{\beta} \frac{1}{\varepsilon_c - \varepsilon_v - \beta(\hbar\omega + i\eta)}$).[9] Where d represents an effective thickness of 2D InSe and S denotes the area in period cell on 2D InSe. In order to investigate the accuracy of the dielectric tensor of 2D InSe, we further investigated the optical properties (including optical absorption spectra (a) and optical reflection spectra (b)) of the 2D InSe, as plotted in Fig. S7. The normalized reflectance ***R*** and absorbance ***A*** are independent of the light polarization for a suspended 2D InSe when normal incidence is assumed, and it holds $R = \left|\frac{\tilde{\sigma}/2}{1 + \tilde{\sigma}/2}\right|^2$ and $A = \frac{Re\tilde{\sigma}}{|1 + \tilde{\sigma}/2|^2}$.[9] Where $\tilde{\sigma}(\omega) = \sigma_{2D}(\omega)/\varepsilon_0 C$ is the normalized optical conductivity (C and ε_0 represent the speed of light and the permittivity, respectively). The more calculation details for the optical properties of the 2D InSe can be seen the post-processing tool VASPKIT. By comparison, we can find that our absorption for the 2D InSe is supported by previous experimental measured and theoretical results.[11-13]

Table. S1 The Born effective charge Z^*, dielectric constant ε of 2D InSe under the different electric fields.

E (V/Å)	Atom	$Z^*_{xx} = Z^*_{yy}$	Z^*_{zz}	$\varepsilon_{xx} = \varepsilon_{yy}$	ε_{zz}
0	Se In	-2.44 2.44	-0.24 0.27	3.34	1.41
0.006	Se In	-2.42 2.44	-0.16 0.17	3.32	1.28

0.02	Se In	-2.41 2.45	-0.17 0.17	3.32	1.28
0.1	Se In	-2.39 2.55	-0.16 0.17	3.33	1.29
0.3	Se In	-2.24 2.65	-0.15 0.15	3.46	1.30

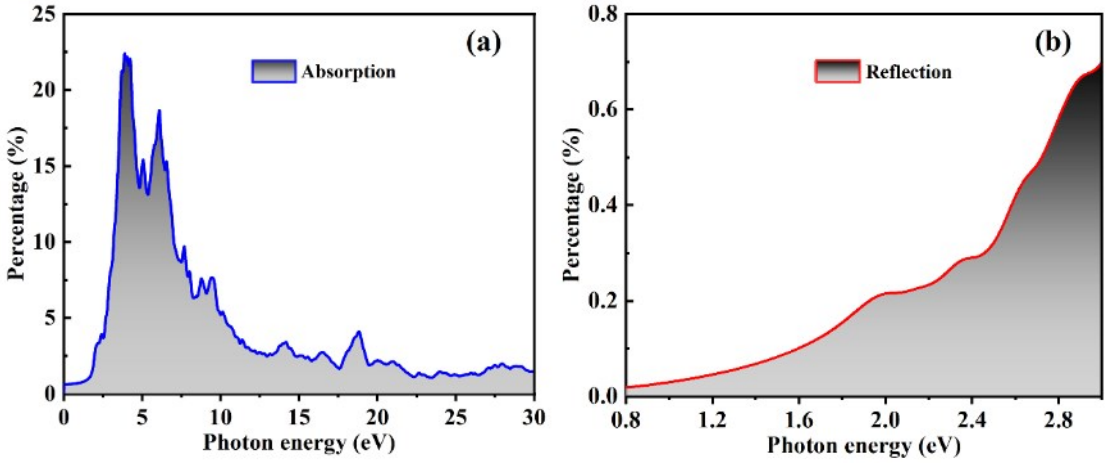

Fig. S7 The optical absorption spectra (a) and optical reflection spectra (b) of 2D InSe under the external electric field of 0 V/Å.

We used parabolic band approximation method to compute the effective mass of 2D InSe, and some figures with calculation details are shown in Fig. S8.

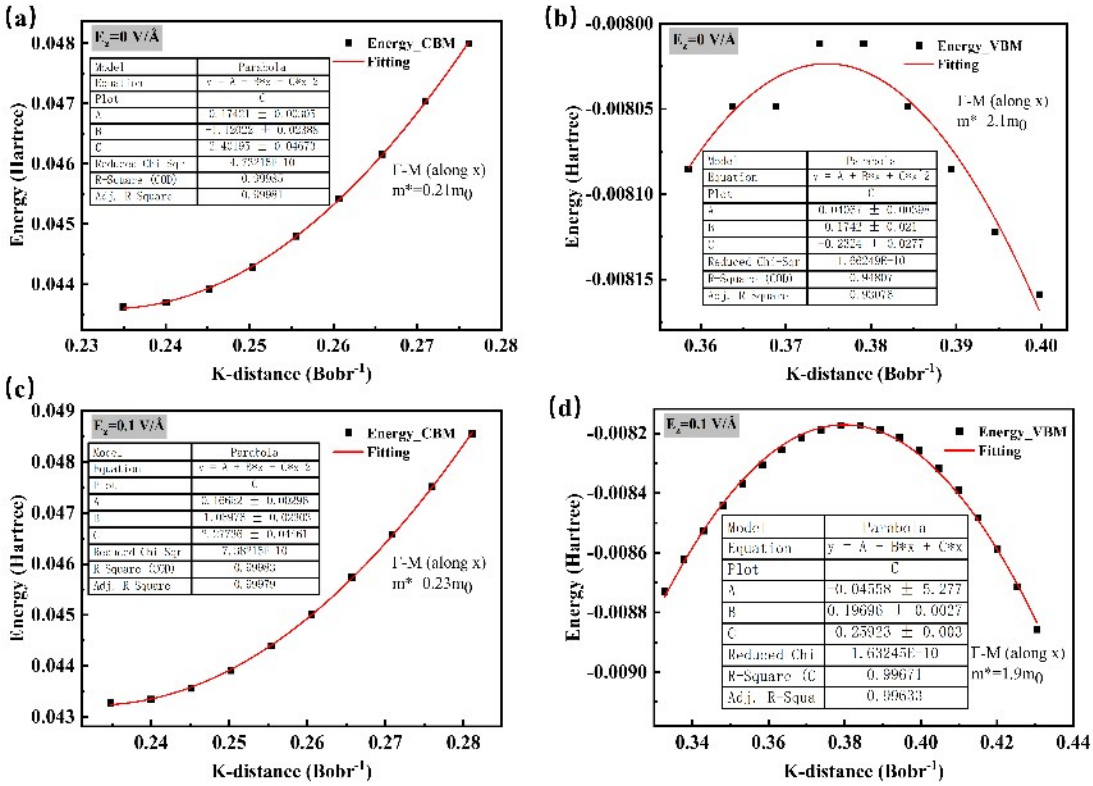

Fig. S8. The effective mass (m^*) of 2D InSe along the x (y) direction under the external electric field of 0 and 0.1 V/Å, computed as $m^* = \hbar^2\left(\partial^2 E/k^2\right)^{-1}$ by parabolic curve fitting the conduction band minimum and the valence band maximum to a quadratic function.

To obtain the deformation potential constant, the absolute band edge is calculated by $E_{CBM/VBM}^{Abs} = E_{CBM/VBM}^{DFT} - E_{Vacuum}$, where $E_{CBM/VBM}^{DFT}$ is the eigenvalue of CBM/VBM obtained from the DFT calculation and E_{Vacuum} represents the electrostatic potential in the vacuum region.[14] Fig. S9 shows the absolute band edge of the valence band of the 2D InSe versus lattice change along the *x* or *y* direction under different values of applied electric fields.

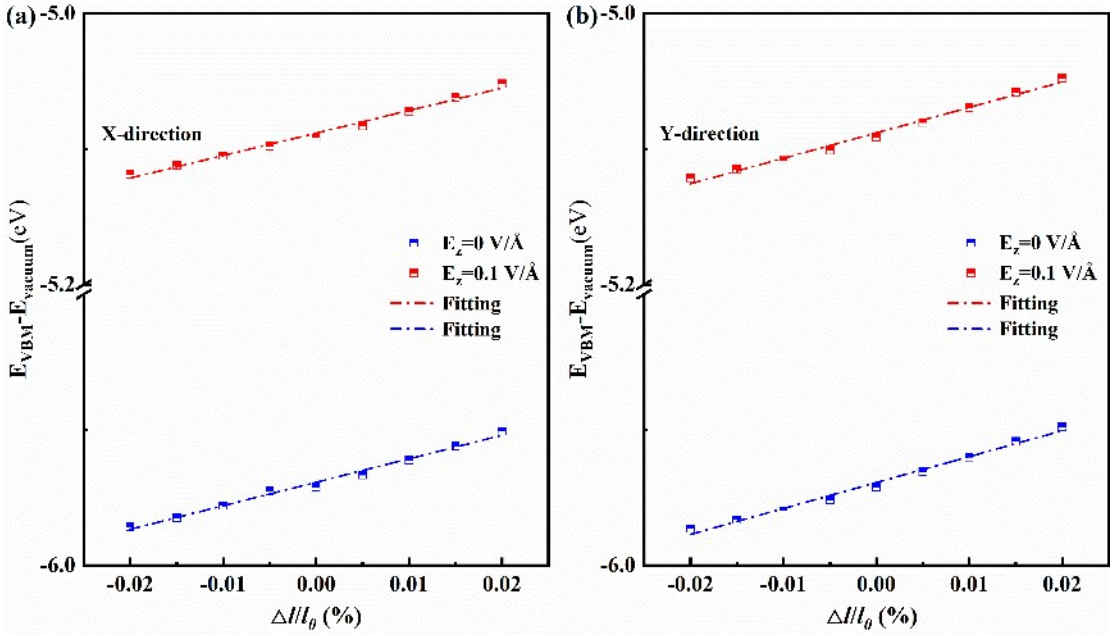

Fig. S9. The absolute band edge of the valence band of the 2D InSe versus lattice change along the x or y direction under different values of applied electric fields (0.0 V/Å, 0.1 V/Å).

To eliminate the missing information in Fig. 11, we added more detailed anisotropic square of group velocities, as shown in Fig. S10. We want to express that the phonon group velocity has weak anisotropy in the presence of an external electric field and zero field cases.

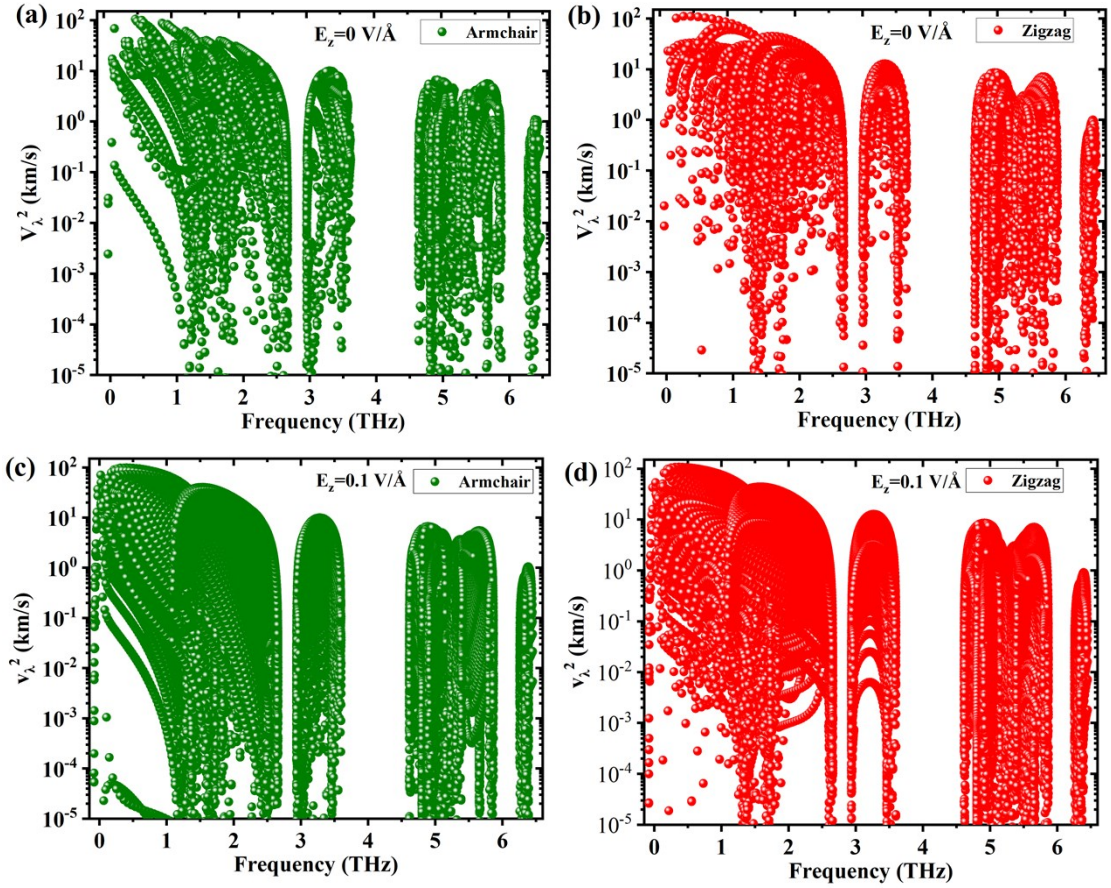

Fig. S10 Anisotropic square group velocity as a function of frequency for 2D InSe under the external electric field of (a-b) 0 and (c-d) 0.1 V/ Å, respectively.

In order to further examine the almost no changed group velocities of 2D InSe under different external electric fields, we plot the group velocities of three acoustic modes in some representative electric fields as shown in Fig. S11. Here, we also calculate the group velocities of the phonon mode ω_i using the slope of the phonon dispersion for the five external electric fields, which are given by

$$v_{i,q} = \frac{\partial \omega_{i,q}}{\partial q} . \tag{S1}$$

Fig. S11 highlights the acoustic phonon group velocities for the TA, LA and ZA branches with black, red and blue lines, respectively. The different shapes of the acoustic phonon dispersion will lead to different group velocities v_q for 2D InSe applying with different electric fields at the high-symmetry paths zone. As shown in Fig. S11, with increasing the electric field from 0 to 0.3 V/Å, the group velocities of three acoustic phonon branches for 2D InSe changes slightly and indicating that the

harmonic effect does not have the dominant role.

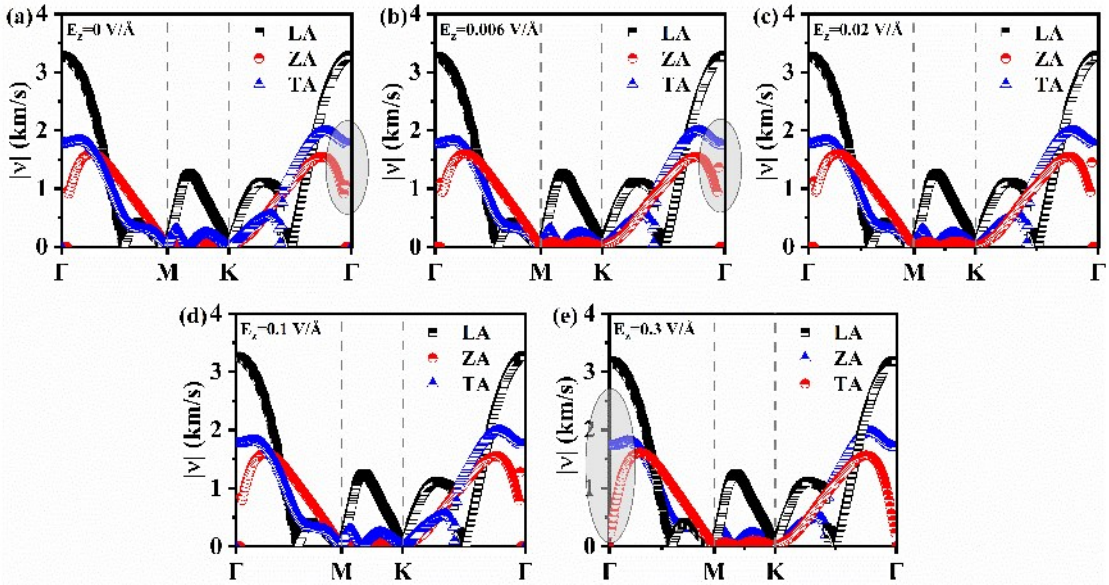

Fig. S11. Calculated group velocities of 2D InSe three acoustic phonon modes along the high-symmetry paths for (a) E_z=0.0 V/Å, (b) E_z=0.006 V/Å, (c) E_z=0.02 V/Å, (d) E_z=0.1 V/Å and (e) E_z=0.3 V/Å.

From Fig. S12, It can be noticed that the rapid increase in the specific heat is marked feature of these cases, and when the temperature reaches to 800 K, specific heat capacity saturates constant following the Dulong-Petit law. At 300 K, the specific heat capacities of model with E_z=0, 0.1 V/Å and E_z=0.3 V/Å are 96.33, 96.34 and 96.46 (J $K^{-1}mol^{-1}$), respectively.

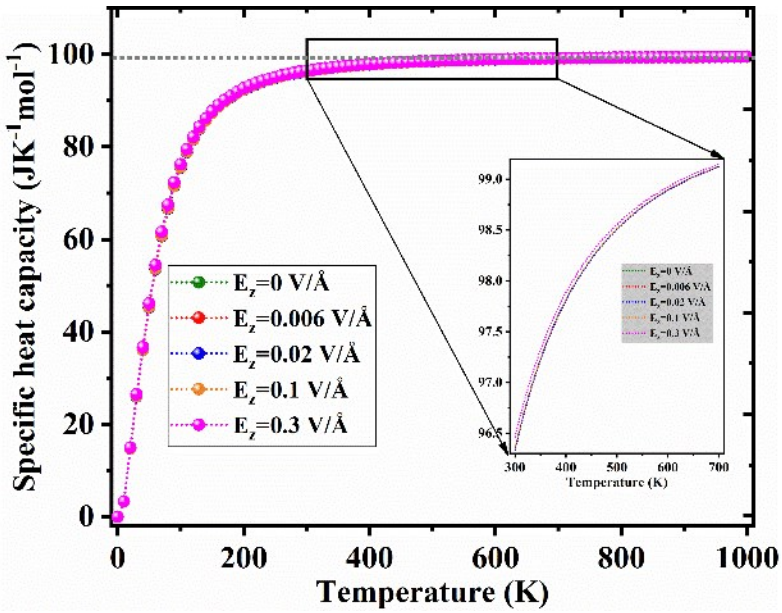

Fig. S12. Variation in specific heat capacity of 2D InSe under some representative electric fields with temperature. The difference in magnitude at the temperature range of 300 K to 700 K is shown in the inset.

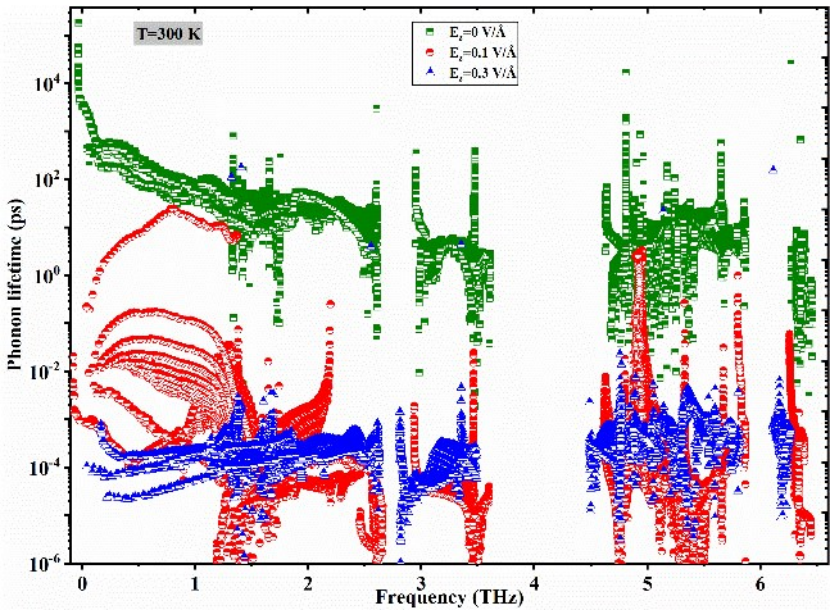

Fig. S13. Phonon lifetime of 2D InSe at room temperature under some representative electric fields.

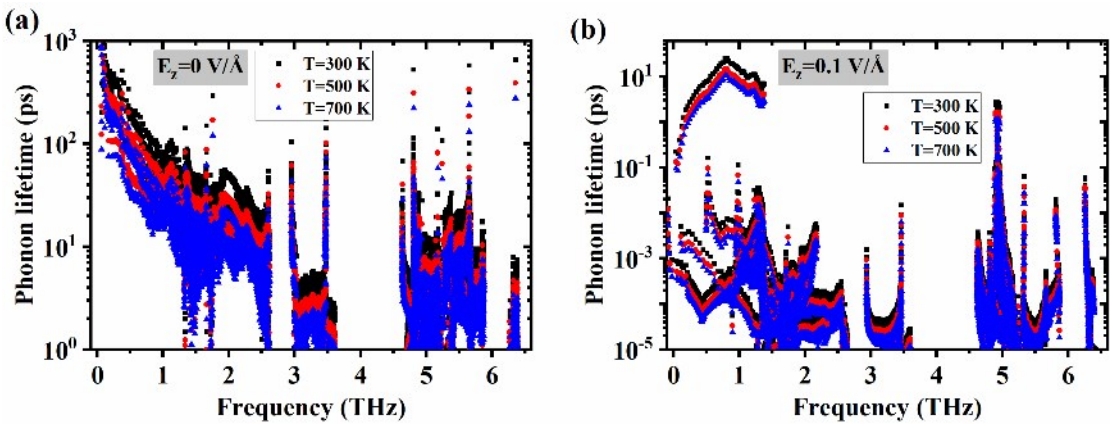

Fig. S14. (a) The phonon lifetime versus frequency for T=300, 500 and 700K at the electric field of 0 V/Å. (b) The phonon lifetime versus frequency for T=300, 500 and 700K at the electric field of 0.1 V/Å.

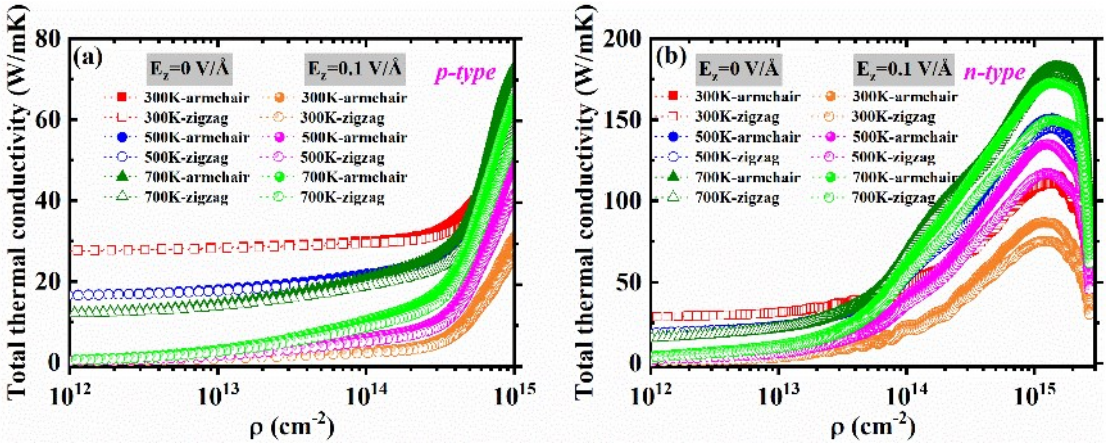

Fig. S15. The total thermal conductivity along armchair and zigzag direction with different carrier concentration under the electric field of 0 and 0.1 V/Å at 300 K, 500 K and 700 K for (a) *p-type* and (b) *n-type* 2D InSe.

References

1. S. Nosé, *The Journal of chemical physics*, 1984, **81**, 511-519.
2. O. I. Malyi, K. V. Sopiha and C. Persson, *ACS applied materials & interfaces*, 2019, **11**, 24876-24884.
3. G. Qin, Z. Qin, H. Wang and M. Hu, *Computational Materials Science*, 2018, **151**, 153-159.
4. S. Lee, K. Esfarjani, T. Luo, J. Zhou, Z. Tian and G. Chen, *Nature communications*, 2014, **5**, 1-8.
5. C. Liu, P. Lu, Z. Gu, J. Yang and Y. Chen, *The Journal of Physical Chemistry C*, 2020.
6. V. Wang, N. Xu, J. C. Liu, G. Tang and W.-T. Geng, *arXiv preprint arXiv:1908.08269*, 2019.
7. H. Zhou, Y. Cai, G. Zhang and Y. W. Zhang, *Nanoscale*, 2017, **10**, 480-487.
8. A. Shafique and Y.-H. Shin, *Scientific reports*, 2020, **10**, 1-10.
9. L. Matthes, O. Pulci and F. Bechstedt, *Physical Review B*, 2016, **94**, 205408.
10. F. Bechstedt and R. Enderlein, *Superlattices and Microstructures*, 1986, **2**, 543-549.
11. Y. He, M. Zhang, J.-j. Shi, Y.-l. Cen and M. Wu, *The Journal of Physical Chemistry C*, 2019, **123**, 12781-12790.
12. C. Song, F. Fan, N. Xuan, S. Huang, C. Wang, G. Zhang, F. Wang, Q. Xing, Y. Lei and Z. Sun, *Physical Review B*, 2019, **99**, 195414.
13. R. Damon and R. Redington, *Physical Review*, 1954, **96**, 1498.
14. W.-B. Zhang, L.-J. Xiang and H.-B. Li, *Journal of Materials Chemistry A*, 2016, **4**, 19086-19094.